Research Article

Synthesis and Magnetorheology Study of Iron Oxide and Iron Cobalt Oxide Suspensions

Syang-Peng Rwei,[1] Lee Yi Wang,[2] and Po-Wen Yang[1]

[1] *Institute of Organic and Polymeric Materials, National Taipei University of Technology, No. 1, Section 3,*
  Chung-Hsiao E. Road, Taipei 10648, Taiwan
[2] *Center Condensed Matter Science, National Taiwan University, Taipei, Taiwan*

Correspondence should be addressed to Syang-Peng Rwei; f10714@ntut.edu.tw

This study investigates the magnetorheology (MR) of polydimethylsiloxane (PDMS) that contains magnetic powders of various compositions, shapes, and concentrations. Two magnetic powders, Fe_3O_4 and $CoFe_2O_4$, were synthesized. TEM images reveal that a powder of spherical particles was obtained at high temperature. A powder with nonspherical star shape was synthesized at low temperature. A rheological test confirmed a typical Bingham behavior for all the MR fluids prepared in this study. Experimental results demonstrated that the cobalt ferrite exhibited a more superior yield stress than the ferrite compound. A magnetic powder of larger particles was found to have higher yield stress. Moreover, the spherical particles yielded a higher yield stress than the star-shaped particles. The "saturated magnetic strength" increased with the loading of the magnetic powder. Finally, the results demonstrate that 12 wt% $CoFe_2O_4$ nanopowder (10 nm) dispersed in the PDMS liquid exhibited a large range of yield stresses (0 to 644 Pa).

1. Introduction

A magnetorheological (MR) fluid can be rapidly transformed from a Newtonian fluid-like structure to a solid-like structure with viscoelastic-plastic yielding by applying a magnetic field [1–7]. Rabinow [8] discovered this phenomenon in 1948. Since then, various metal or ceramic powders with magnetic characteristics have been dispersed in nonmagnetic carrier liquids [9], such as oil or aqueous liquids, in the preparation of MR fluids. The smart damper design [10] is currently the most advanced application of MR suspensions. It releases energy using a magnetorheological dashpot and uses electric power to align magnetic nanoparticles that are suspended in liquid with a magnetic warp. The particles are orientated almost perpendicular to the direction of fluid motion (Figure 1). Accordingly, the flow is blocked and the viscosity is thus increased. Regardless of the magnitude of a shock, the energy dissipation always remains optimal in the smart damper because the viscosity of the suspension can be adjusted.

Among all the methods to produce the magnetic nano-particles [11–13], the thermal decomposition method was the most common one in a lab scale and was therefore selected in this work. This study investigates the magnetic fluids, with a view to form magnetic nanoparticles of different shapes and sizes under the control of chemosynthesis [14–18] and then to mix them with PDMS to make magnetic fluid with various solid loadings. MR tests are then performed. The most common MR fluid consists of particles on a micron-scale, normally 5–200 μm in size. The micron-scale particles are too weak to be stabilized by the Brownian motion, and, using which, the reproducibility of MR characterization is difficult to achieve. Accordingly, the sedimentation of particles remains a critical problem to solve in relation to most designed MR fluids—even those that involve added surfactants. Nanoparticles, however, can be easily stabilized in a liquid with the aid of Brownian motion and the repulsive effect from the surfactant. A special synthetic approach was followed in this study to produce nanoscale particles in a manner that eliminates the sedimentation problem.
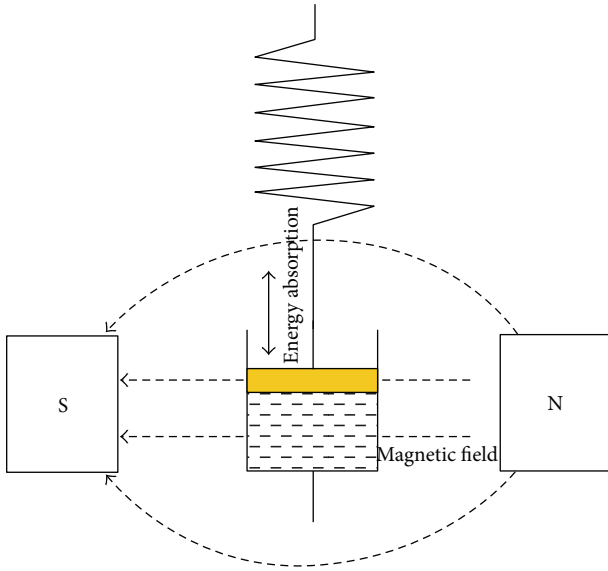
Figure 1: Schematic diagram of magnetorheological damper [19].

2. Experimental

2.1. Preparation of Iron Oxide (Fe_3O_4) Nanoparticles. $FeCl_3 \cdot H_2O$ (10.8 g, 40 mmol), sodium oleate (36.5 g, 120 mmol), distilled water (60 mL), ethanol (80 mL), and hexane (140 mL) were put in a 500 mL three-neck flask and stirred under nitrogen for one hour to dissolve them completely. Then, the flask was mounted onto a condensing system and heated to 70°C at a heating rate of 3.3°C/min in the nitrogen environment. This temperature was maintained for 4.5 hours and three extractions were performed after the reaction using distilled water (60 mL). The iron-oleate complex (1) with a black-brown appearance was obtained. A rotary concentrator was then used to remove the solvent.

Product (1) (9.00 g, 10 mmol), oleic acid (1.73 g, 6 mmol) and tri-n-octylamine (30.00 g) were put in a 500 mL three-neck flask. A magnet was added and stirred in a nitrogen environment for 40 minutes to mix the contents uniformly. The condensing system, in the nitrogen environment, was set up to 300 or 366°C at a heating rate of 3.3°C/min. A black solution was obtained after reaction for 30 minutes. The ethanol was used to separate out the black solid, namely, the Fe_3O_4 product. Finally, the Fe_3O_4 was purified using hexane to remove the organic substance on its surface (Figure 2).

2.2. Preparation of Iron Cobalt Oxide ($CoFe_2O_4$) Nanoparticles. The cobalt ferrite nanoparticles have been prepared using the method developed by Hyeon as follows [20]. Iron (III) acetylacetonate (0.71 g, 2 mmol), cobalt (II) acetylacetonate (0.26 g, 1 mmol), and 1,2-tetradecanediol (2.56 g, 10 mmol) were put in a 500 mL three-neck flask. Nitrogen deoxidized phenyl ether (20 mL), oleic acid (1.73 g, 6 mmol), and oleyamine (2.00 g, 6 mmol) were then added and stirred in a nitrogen environment for one hour to ensure uniform mixing. The condensing system, in the nitrogen environment, was set up to 200°C at a rate of 3.3°C/min and maintained

for 30 minutes; the system was then heated to 265°C at a heating rate of 3.3°C/min and maintained for 30 minutes. Alternatively, the condenser was heated to 300°C and maintained for one hour after reaction at 200°C for two hours. A black solution was yielded after the reaction is complete and ethanol was used to separate out the black solid. The black solid thus obtained is the product $CoFe_2O_4$. The $CoFe_2O_4$ was purified using hexane to remove the organic substance on its surface (Figure 3). All of the chemicals used were supplied by ACROS Chemicals and used without further purification.

2.3. Preparation of Magnetic Fluid. The magnetic material 0.2 g was blended with 1.5 mL polydimethylsiloxane (PDMS, viscosity 100 cp) and stirred uniformly. The content was poured into the lower plate of rheometer (Anton Paar Physica MCR301 MRD). Then, the upper plate was lowered to maintain the spacing between the plates at 0.1 cm. The temperature of the rheometer was kept at 25°C. The yield stress of the object was measured under various magnetic strength. The samples were prepared in the following orders: (1) Fe_3O_4 (300°C), (2) Fe_3O_4 (366°C), (3) $CoFe_2O_4$ (265°C), and (4) $CoFe_2O_4$ (300°C).

2.4. Principle of Magnetorheology. Figures 4(a) to 4(d) present the basic principle of magnetorheology. When a magnetic fluid is placed in a magnetic field, magnetic nanoparticles are temporarily in a network state, as shown in Figures 4(b) to 4(c). The purpose of shear test is to determine the critical shear stress, also known as the yield stress, which disrupts the network state (Figure 4(d)). A larger yield stress indicates that the tested MR fluid exhibits a stronger MR effect.

The pure PDMS fluid that was used herein is a Newtonian fluid. An MR fluid, in contrast, exhibits Bingham character in a magnetic field. Such a Bingham fluid [19] has a so-called yield stress (τ_0). The MR fluid must overcome this threshold for the onset of fluidity in a magnetic field. Equation (1) defines "apparent viscosity" (μ_a), taking into account the yield stress in viscosity calculation.

$$\tau = \tau_0 + \mu_0 \dot{\gamma},$$
$$\mu_a = \frac{\tau}{\dot{\gamma}} = \frac{\tau_0}{\dot{\gamma}} + \mu_0. \tag{1}$$

In (1), τ denotes the shear stress; τ_0 denotes the yield stress; μ_0 denotes the quasi-Newtonian viscosity; $\dot{\gamma}$ represents the shear rate, which is the gradient of the velocity against the vertical displacement, and μ_a represents the apparent viscosity, which is the ratio of the measured shear stress to the given shear rate.

For a fixed shear rate, a larger yield stress corresponds to a higher apparent viscosity. The magnetic field is adjusted by varying the electric current, and the targeted apparent viscosity is thereby obtained.

3. Results and Discussion

Figure 5(a) presents the wide-angle X-ray diffraction pattern of Fe_3O_4 particles that were synthesized in this work. All of
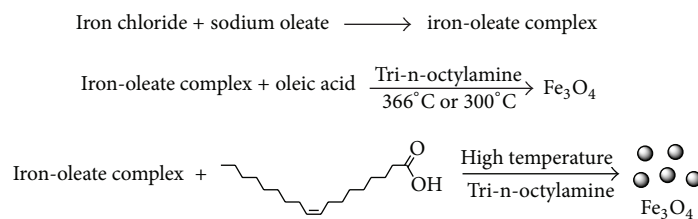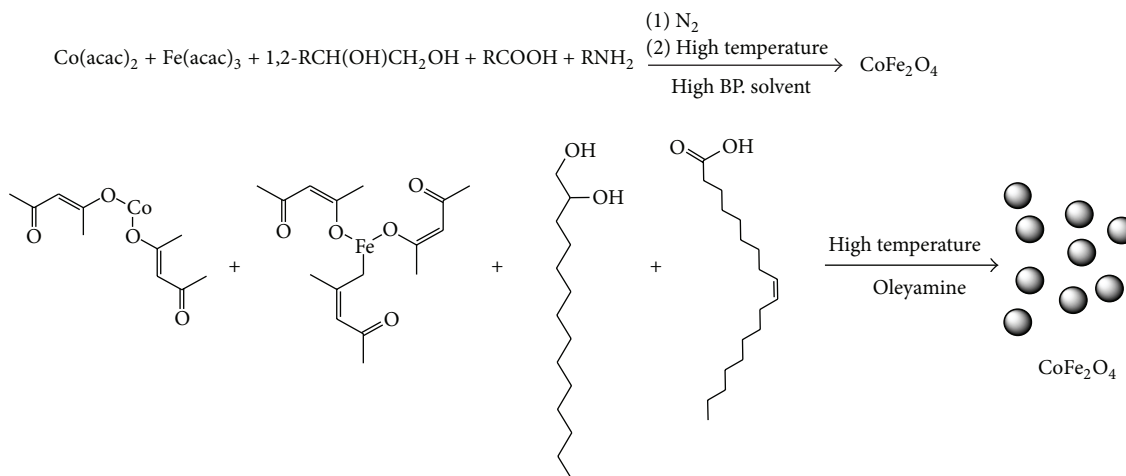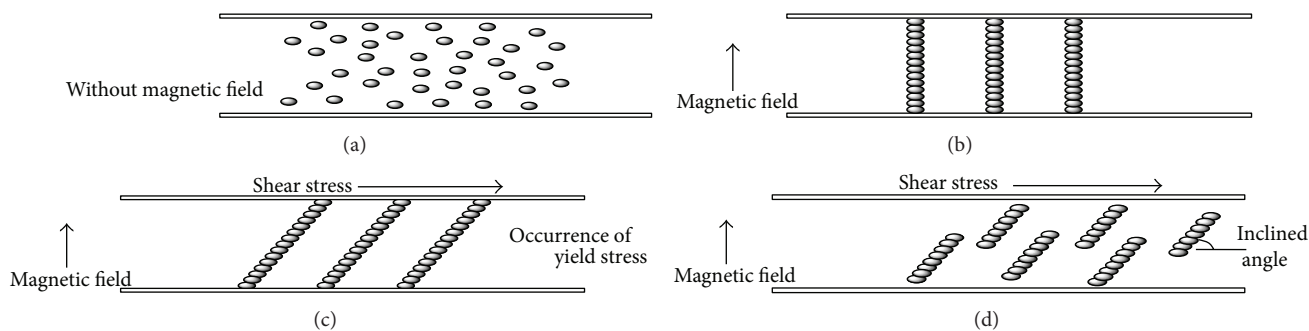
Iron chloride + sodium oleate $\longrightarrow$ iron-oleate complex

Iron-oleate complex + oleic acid $\xrightarrow[366°C \text{ or } 300°C]{\text{Tri-n-octylamine}}$ Fe$_3$O$_4$

Iron-oleate complex + [structure] $\xrightarrow[\text{Tri-n-octylamine}]{\text{High temperature}}$ Fe$_3$O$_4$

FIGURE 2: Scheme of Fe$_3$O$_4$ nanoparticle Synthesis.

Co(acac)$_2$ + Fe(acac)$_3$ + 1,2-RCH(OH)CH$_2$OH + RCOOH + RNH$_2$ $\xrightarrow[\text{High BP. solvent}]{\substack{(1)\ N_2 \\ (2)\ \text{High temperature}}}$ CoFe$_2$O$_4$

[chemical structures] $\xrightarrow[\text{Oleyamine}]{\text{High temperature}}$ CoFe$_2$O$_4$

FIGURE 3: Preparation of iron cobalt oxide (CoFe$_2$O$_4$) nanoparticles.

(a)

(b)

(c)

(d)

FIGURE 4: Schematic diagram of yield stress.

the characteristic peaks of the crystal (30.1 (200), 35.4 (311), 37.0 (222), 43.1 (400), 53.4 (422), 56.9 (511), 62.5 (440)) are similar to other scholars' results [21, 22], proving that the synthesized particles are granular Fe$_3$O$_4$ crystals. The wide-angle X-ray diffraction pattern of CoFe$_2$O$_4$ particles that were synthesized in this work was shown in Figure 5(b). All of the characteristic peaks (18.1 (111), 30.1 (220), 35.7 (311), 37.0 (222), 43.1 (400), 53.4 (422), 57.0 (511), 62.5 (440)) of the crystal are similar to other scholars' results [23–25], indicating that the synthesized particles are granular CoFe$_2$O$_4$ crystals.

Figures 6(a) and 6(b) are TEM photos of Fe$_3$O$_4$ particles that were synthesized at 366°C and 300°C, respectively. They reveal that the particles formed at 300°C are star shaped; the

longest diagonal distance between two apexes is 80 nm, and the internal diameter of the particles is around 40 nm. In contrast, regular, spherical particles (30 nm in diameter) are obtained at 366°C, suggesting that a high temperature yields round and uniform particles, and a low temperature yields nonspherical particles, even with multi-acute angles.

Crystallization is usually divided into "nucleation" and "growth" stages. Low temperature favors nucleation but is disadvantageous to growth, whereas high temperature disfavors nucleation but favors growth. The reactant diffusion rate is low at low temperature. The crystal nucleus is unlikely to grow uniformly to form a 3-D symmetrical sphere; in contrast, particles with polygonal shape are synthesized. The convex
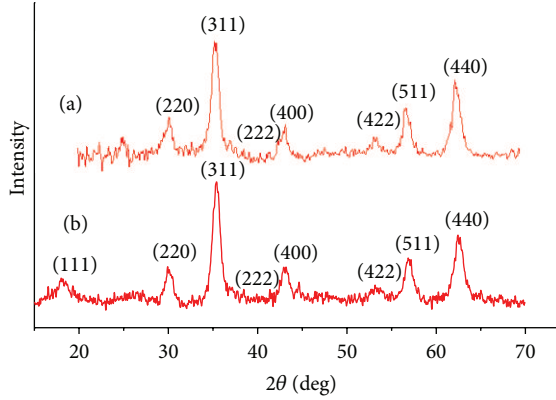
FIGURE 5: X-ray diffraction pattern of (a) Fe_3O_4 and (b) $CoFe_2O_4$.

TABLE 1: Various shapes and sizes of nanoparticles synthesized at different temperatures.

Particle type	Synthesis temperature (°C)	Shape	Diameter (nm)
Fe_3O_4	300	Star	$40 \pm 6^*$
Fe_3O_4	366	Sphere	30 ± 2
$CoFe_2O_4$	265	Sphere	3 ± 1
$CoFe_2O_4$	300	Sphere	10 ± 3

*The mean value of the core-diameter of the star particles.

TABLE 2: The τ_{0a} and μ_0 of $CoFe_2O_4$ 12 wt% MR fluid under different magnetic strengths.

Magnetic field strength (Gauss)	τ_{0a} (Pa)	μ_0 (Pa S)
0	0	0.5
1400	296.8	0.9
2800	404.3	1.2
5800	511.5	1.4
8600	576.7	1.5
10000	644.3	1.6

surfaces of a polygonal particle can more easily capture a new Fe_3O_4 ionic particle than can do the spherical surfaces, so the crystal keeps growing along the convexity and forms several arms. Therefore, star-shaped particles with multiacute angles are formed. However, the diffusion rate is high at high temperature, and the crystal nuclei are uniform, so numerous new Fe_3O_4 ionic particles are stratified on the surface of each nucleus simultaneously. The crystallization time is too short to allow any nucleus to form a convexity, so round crystals uniformly grow instead. The formation of the star-shaped or polygonal nanoparticles was also observed by other scholars [26, 27], and similar growth mechanism was proposed.

Figures 6(c) and 6(d) are the TEM images of $CoFe_2O_4$ particles that were synthesized at 265°C and 300°C, respectively. Particles that were synthesized at high temperature were spherical with a relatively uniform diameter of approximately 10 nm. Particles synthesized at low temperature, however, are nonspherical and have sizes of 3~5 nm. The difference between the shapes of $CoFe_2O_4$ particles can be explained similarly to the mechanism of formation of the Fe_3O_4 particles mentioned previously; a high temperature promotes the formation of round particles because the rate of the diffusion of the ionic particles is high enough to make the suspension contain a homogenous ionic-particle distribution at high temperature. At higher temperatures, nucleation and growth may not be easily separated. The homogeneity of the crystallization process is better and can thus yield a more spherical particle with a larger diameter. The relationship between synthesis temperature and the shape of $CoFe_2O_4$ and Fe_3O_4 particles is shown in Table 1. Notably, the dependence of temperature on particle size and shape is only valid for the "thermal decomposition method" used herein. Similar result was also reported by other scholars [28].

Figure 7 presents the MR result of $CoFe_2O_4$ (synthesized at 300°C) dispersed in PDMS (12 wt%). The MR fluid clearly changed from a Newtonian fluid to a Bingham fluid when a magnetic field was applied. As the magnetic field increases, the yield stress (τ_0) increases, and the quasi-Newtonian viscosity (μ_0) of the fluid increases. Table 2 summarizes the results from Figure 7. Table 2 demonstrates that the yield stress, defined as the extrapolated stress at zero shear rate,

increases with the magnetic field. Accordingly, when the magnetic field increases, the magnitude of the yield stress, which is the range of deformation before fracture, increases, as demonstrated in Figure 4(c). If the line of magnetic nanoparticles is broken, then various dispersed particle groups advance in the original direction of the shear force and thus flow forward. However, the magnetic field causes the particle groups to follow an inclination that deviates from the direction of flow in the flow process. A larger deviation corresponds to greater resistance of the fluid and, therefore, a greater viscous stress. Therefore, quasi-Newtonian viscosity (μ_0) increases with magnetic force. In fact, the Bingham yield stress (τ_0) and quasi-Newtonian viscosity (μ_0) do not increase without limit. When the magnetic field continues to increase, the magnetic fluids eventually reach their own "saturated magnetic strength."

Figure 8 plots the relationship between yield stress (τ_0) and magnetic flux density (G) for Fe_3O_4 (366°C) fluid at various concentrations. Evidently, the yield stress increases with the magnetic field. However, the saturated magnetic strength, which the yield stress does not further increase after the magnetic force is raised over, can be obtained for the Fe_3O_4 suspension at a low concentration. Figure 8 reveals that the saturated magnetic strengths of 3 wt% and 6 wt% Fe_3O_4 fluids are 6000 G and 8600 G, respectively. However, the saturation point of 12 wt% Fe_3O_4 is far beyond the measurable range (10000 G) of the instrument, so it cannot be determined. In summary, Figure 8 demonstrated that the saturated magnetic strength increases with the particle concentrations.

Figure 9 plots the shear stress against shear rate for magnetic nanoparticles with different shape, size, and species. Figure 9 plots the effect of size on the MR behavior of $CoFe_2O_4$ particles of similar shapes (spherical or almost spherical). $CoFe_2O_4$ particles with a diameter of 10 nm have
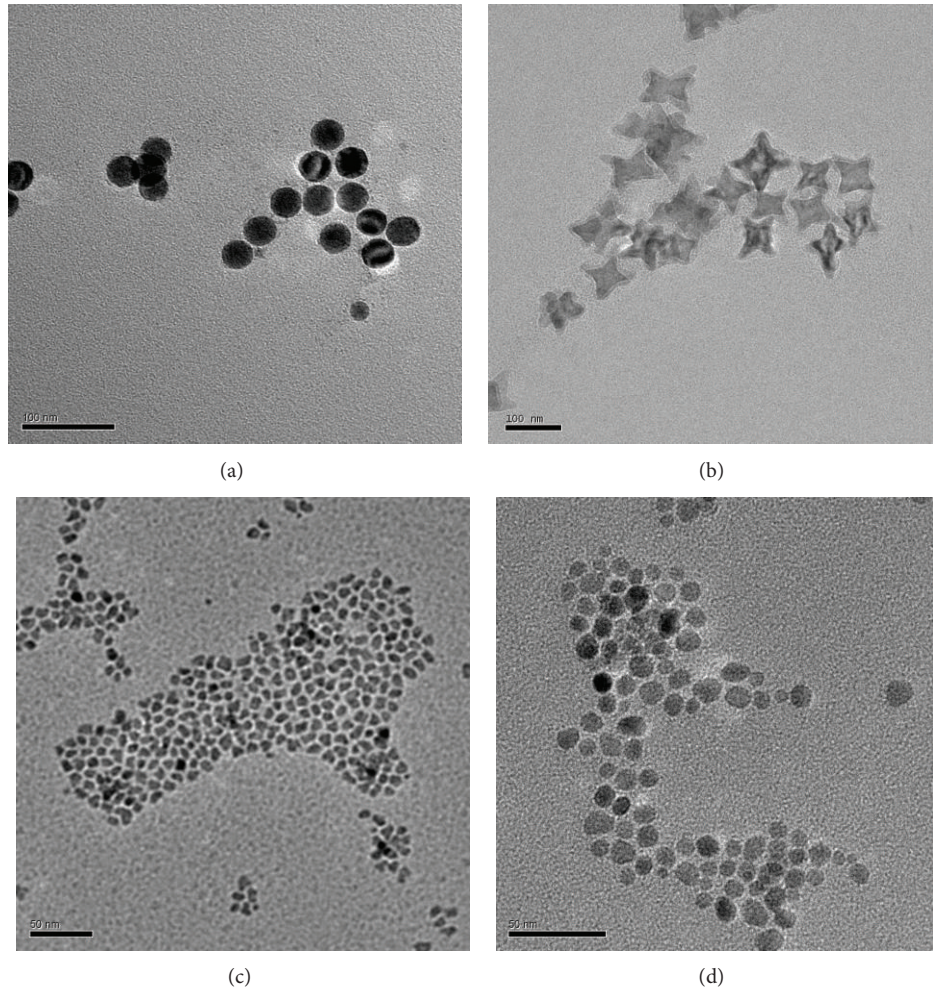
(a)

(b)

(c)

(d)

FIGURE 6: TEM photographs of (a) Fe_3O_4 particles synthesized at 366°C, (b) Fe_3O_4 particles synthesized at 300°C, (c) $CoFe_2O_4$ synthesizing particles at 265°C, and (d) $CoFe_2O_4$ synthesizing particles at 300°C.
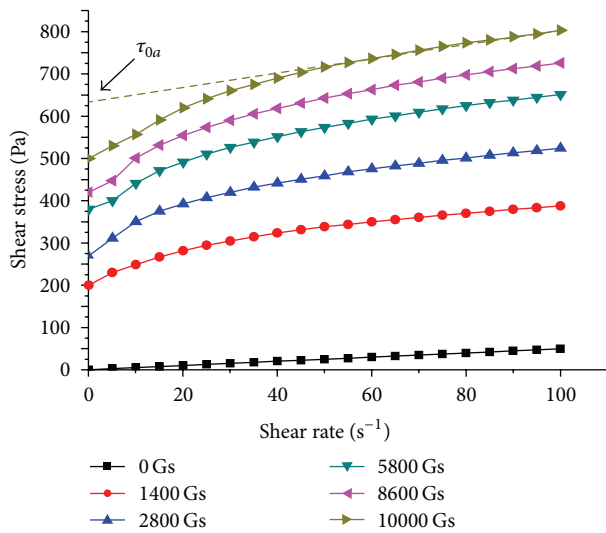

FIGURE 7: Shear stress is a function of shear rate for $CoFe_2O_4$ particles, synthesized at 300°C, under various magnetic fields.
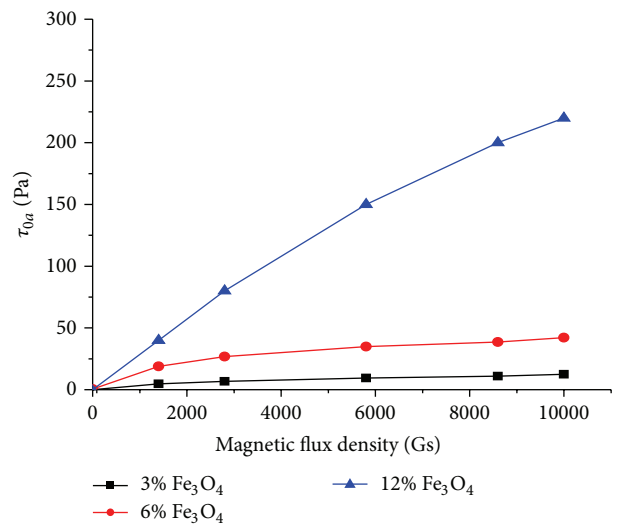

FIGURE 8: The yield stress of Fe_3O_4 fluid at different solid loading (366°C) as a function of magnetic flux intensity (Gauss).
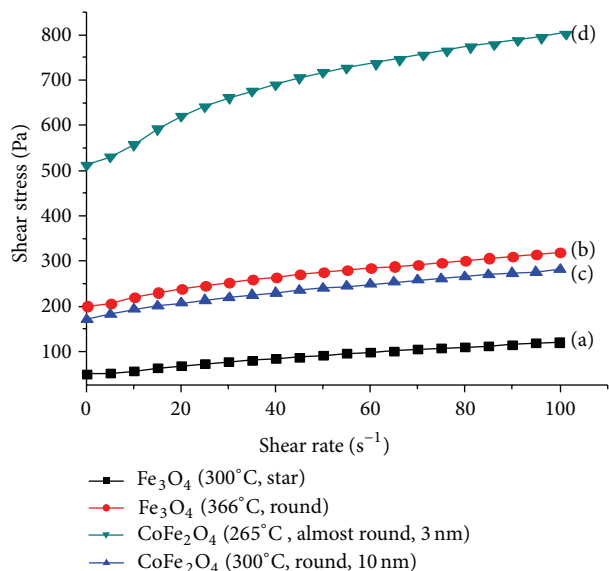
FIGURE 9: Shear stress against shear rate for various magnetic nanoparticles dispersed in silicone oil (10000 Gauss, 25°C, 12 wt%).
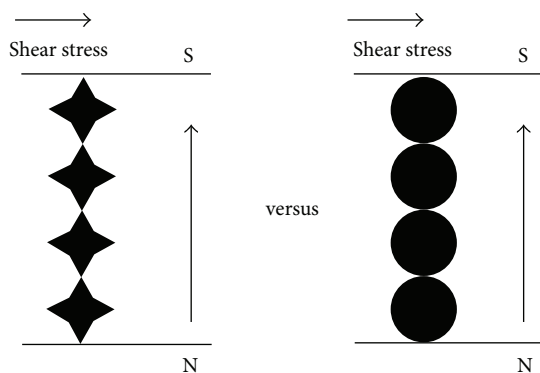

FIGURE 10: Effect of shear stress and magnetic force on star-shaped and round particles.

the best yield stress, 644 Pa, and quasi-Newtonian viscosity, 1.6 Pa S. $CoFe_2O_4$ particles with a smaller diameter, 3 nm, have a poor yield stress, which is only one third of that of the larger panicles, 188 Pa. Theoretically, a larger particle has fewer connection points and is unlikely to be destroyed by shear stress. Therefore, it can exhibit a higher MR yield stress. Figure 9 demonstrates that the yield stress of the $CoFe_2O_4$ series clearly exceeds that of the Fe_3O_4 series, indicating that the magnetic strength of iron cobalt oxide exceeds that of iron oxide [29]. The incorporation of the Co cation in the Fe-O matrix greatly increases the magnetic anisotropy of the materials, resulting in higher coercivity. Ferromagnetic materials with high coercivity have permanent magnets which can sustain a harsh and complex hydrodynamic environment and yield a good MR behavior. The drawback of the particles with high coercivity is the problem of particle dispersion when the field is out [30, 31]. How to prepare an MR fluid with high

magnetic strength but low self-flocculation is a tough task for us in the future.

Figure 10 illustrates that a round particle of Fe_3O_4 has a higher yield stress than a star particle. The core diameter of the star particle (40 nm) exceeds the diameter of the round particle (30 nm). According to the results for ferrocobalt oxide, larger particles are associated with higher yield stress, but the experiment to which Figure 9 pertains yields the opposite result. The junction of the star-shaped particle may be the connection between two arms, and it is less stable than the connection of two round particles. Accordingly, this fragile joint is easy to be destroyed by a shear force, resulting in a reduced yield force.

4. Conclusions

Fe_3O_4 is likely to be synthesized at high temperature (366°C) as round uniformly sized particles, and at low temperature (300°C) as star-shaped particles. Based on the MR test results, we conclude the following.

(1) The yield stress of the $CoFe_2O_4$ fluid is three to ten times higher than that of Fe_3O_4 fluid at the same concentration.

(2) In an MR fluid of round $CoFe_2O_4$ particles larger particles produce higher yield stress.

(3) The yield stress of MR fluid with round particles exceeds that of such a fluid with star-shaped particles.

(4) In an MR test, the "saturated magnetic strength" increases with the particle concentration.

Disclosure

The MR fluids are prepared according to the method mentioned herein as a novel method. Although it still has long way to go for commercial application, its patents have been claimed and filed by the authors and the financial founder: NSC of Taiwan. There is no conflict of interests for any commercial application at present time or in the future.

Acknowledgment

References

[1] I. Bica, "Influence of the transverse magnetic field intensity upon the electric resistance of the magnetorheological elastomer containing graphite microparticles," *Materials Letters*, vol. 63, no. 26, pp. 2230–2232, 2009.

[2] J. H. Kim, F. F. Fang, H. J. Choi, and Y. Seo, "Magnetic composites of conducting polyaniline/nano-sized magnetite and their magnetorheology," *Materials Letters*, vol. 62, no. 17-18, pp. 2897–2899, 2008.

[3] W. H. Li, C. Lynam, J. Chen, B. Liu, X. Z. Zhang, and G. G. Wallace, "Magnetorheology of single-walled nanotube dispersions," *Materials Letters*, vol. 61, no. 14-15, pp. 3116–3118, 2007.

[4] C. C. Ekwebelam and H. See, "Using oscillatory shear to probe the effects of bidispersity in inverse ferrofluids," *Korea Australia Rheology Journal*, vol. 19, no. 1, pp. 35–42, 2007.

[5] H. Pu, F. Jiang, and Z. Yang, "Studies on preparation and chemical stability of reduced iron particles encapsulated with polysiloxane nano-films," *Materials Letters*, vol. 60, no. 1, pp. 94–97, 2006.

[6] W. H. Li and X. Z. Zhang, "The effect of friction on magnetorheological fluids," *Korea Australia Rheology Journal*, vol. 20, no. 2, pp. 45–50, 2008.

[7] S. P. Rwei, H. Y. Lee, S. D. Yoo, L. Y. Wang, and J. G. Lin, "Magnetorheological characteristics of aqueous suspensions that contain Fe_3O_4 nanoparticles," *Colloid and Polymer Science*, vol. 283, no. 11, pp. 1253–1258, 2005.

[8] J. Rabinow, "The magnetic fluid clutch," *Transactions of the American Institute of Electrical Engineers*, vol. 67, no. 2, pp. 1308–1315, 1948.

[9] I. Bica, "The influence of the magnetic field on the electrical magnetoresistance of magnetorheological suspensions," *Journal of Magnetism and Magnetic Materials*, vol. 299, no. 2, pp. 412–418, 2006.

[10] R. Stanway, "Smart fluids: current and future developments," *Materials Science and Technology*, vol. 20, no. 8, pp. 931–939, 2004.

[11] S. Chakrabarti, S. K. Mandal, and S. Chaudhuri, "Cobalt doped γ-Fe_2O_3 nanoparticles: synthesis and magnetic properties," *Nanotechnology*, vol. 16, no. 4, pp. 506–511, 2005.

[12] S. K. Mandal, "Fluorescent magnetic emulsion droplets: potential material for multiplexed optical coding of biomolecules," *Journal of Magnetism and Magnetic Materials*, vol. 311, no. 1, pp. 88–91, 2007.

[13] S. K. Mandal, N. Lequeux, B. Rotenberg et al., "Encapsulation of magnetic and fluorescent nanoparticles in emulsion droplets," *Langmuir*, vol. 21, no. 9, pp. 4175–4179, 2005.

[14] H. R. Brand and H. Pleiner, "Origin of the slow wave in a magnetorheological slurry," *Physical Review Letters*, vol. 86, pp. 1385–1385, 2000.

[15] M. Liță, N. C. Popa, C. Velescu, and L. N. Vékás, "Investigations of a magnetorheological fluid damper," *IEEE Transactions on Magnetics*, vol. 40, no. 2 I, pp. 469–472, 2004.

[16] H. Böse, "Viscoelastic properties of silicone-based magnetorheological elastomers," *International Journal of Modern Physics B*, vol. 21, no. 28-29, pp. 4790–4797, 2007.

[17] H. See, C. Joung, and C. Ekwebelam, "Dynamic behavior and yielding of field-responsive particulate suspensions," *International Journal of Modern Physics B*, vol. 21, no. 28-29, pp. 4945–4951, 2007.

[18] R. C. Bell, E. D. Miller, J. O. Karli, A. N. Vavreck, and D. T. Zimmerman, "Influence of particle shape on the properties of magnetorheological fluids," *International Journal of Modern Physics B*, vol. 21, no. 28-29, pp. 5018–5025, 2007.

[19] F. A. Morrison, *Understanding Rheology*, Guernsey, UK, 2001.

[20] T. Hyeon, Y. Chung, J. Park, S. S. Lee, Y.-W. Kim, and B. H. Park, "Synthesis of highly crystalline and monodisperse cobalt ferrite nanocrystals," *Journal of Physical Chemistry B*, vol. 106, no. 27, pp. 6831–6833, 2002.

[21] K. Hayashi, W. Sakamoto, and T. Yogo, "Magnetic and rheological properties of monodisperse Fe_3O_4 nanoparticle/organic hybrid," *Journal of Magnetism and Magnetic Materials*, vol. 321, no. 5, pp. 450–457, 2009.

[22] A. Kida, C. Yamamoto, M. Doi, H. Asano, and M. Matsui, "Magnetoresistance of trilayer films with Fe_3O_4," *Journal of Magnetism and Magnetic Materials*, vol. 272–276, no. 1, pp. e1559–e1561, 2004.

[23] M. M. Rashad, R. M. Mohamed, and H. El-Shall, "Magnetic properties of nanocrystalline Sm-substituted $CoFe_2O_4$ synthesized by citrate precursor method," *Journal of Materials Processing Technology*, vol. 198, no. 1–3, pp. 139–146, 2008.

[24] L. A. García Cerda and S. M. Montemayor, "Synthesis of $CoFe_2O_4$ nanoparticles embedded in a silica matrix by the citrate precursor technique," *Journal of Magnetism and Magnetic Materials*, vol. 294, no. 2, pp. e43–e46, 2005.

[25] D. Maity and D. C. Agrawal, "Synthesis of iron oxide nanoparticles under oxidizing environment and their stabilization in aqueous and non-aqueous media," *Journal of Magnetism and Magnetic Materials*, vol. 308, no. 1, pp. 46–55, 2007.

[26] C. L. Nehl, H. Liao, and J. H. Hafner, "Optical properties of star-shaped gold nanoparticles," *Nano Letters*, vol. 6, no. 4, pp. 683–688, 2006.

[27] C. Yang, J. Wu, and Y. Hou, "Fe_3O_4 nanostructures: synthesis, growth mechanism, properties and applications," *Chemical Communications*, vol. 47, no. 18, pp. 5130–5141, 2011.

[28] W. W. Yu, J. C. Falkner, C. T. Yavuz, and V. L. Colvin, "Synthesis of monodisperse iron oxide nanocrystals by thermal decomposition of iron carboxylate salts," *Chemical Communications*, vol. 10, no. 20, pp. 2306–2307, 2004.

[29] A. Hernando, I. Navarro, C. Prados, D. García, M. Vázquez, and J. Alonso, "Curie-temperature enhancement of ferromagnetic phases in nanoscale heterogeneous systems," *Physical Review B*, vol. 53, no. 13, pp. 8223–8226, 1996.

[30] S.-Y. Zhao, K. L. Don, W. K. Chang, G. C. Hyun, H. K. Young, and S. K. Young, "Synthesis of magnetic nanoparticles of Fe_3O_4 and $CoFe_2O_4$ and their surface modification by surfactant adsorption," *Bulletin of the Korean Chemical Society*, vol. 27, no. 2, pp. 237–242, 2006.

[31] S. Sun, H. Zeng, D. B. Robinson et al., "Monodisperse MFe_2O_4 (M = Fe, Co, Mn) Nanoparticles," *Journal of the American Chemical Society*, vol. 126, no. 1, pp. 273–279, 2004.